J. Am. Chem. Soc. **1997**, *119*, 3765−3772

3765

Structure and Properties of Li+(Cryptand [2.1.1])e−, an Electride with a 1D "Spin-Ladder-like" Cavity-Channel Geometry

Rui H. Huang, Michael J. Wagner,[†] Deborah J. Gilbert,[‡] Kerry A. Reidy-Cedergren, Donald L. Ward, Margaret K. Faber,[§] and James L. Dye*

Contribution from the Department of Chemistry and Center for Fundamental Materials Research, Michigan State University, East Lansing, Michigan 48824

Received November 25, 1996[⊗]

Abstract: The title electride crystallizes in the orthorhombic space group *Pbcn* with $a = 10.060(4)$ Å, $b = 23.134(8)$ Å, $c = 8.380(4)$ Å, and $z = 4$. A second powdered phase of unknown structure, but with rather different properties, forms when rapidly precipitated "seed" powder is used. The crystalline phase contains electron-trapping cavities, each of approximate diameter 4.3 Å, connected in zigzag fashion along the *c* axis by rather open channels of minimum diameter 2.4 Å (center-to-center distance 7.9 Å). Each cavity is also connected to next-neighbor cavities, 8.2 Å away along *c*, by channels of diameter 1.5 Å. Inter-chain channels are <1.0 Å in diameter so that the cavity-channel structure is well-described as "ladder-like". Replacing the trapped electron by Na− in the corresponding sodide, Li+ (cryptand [2.1.1])Na−, results in an orthorhombic structure (space group *Pna*2₁). Although the anionic sites in the sodide are only slightly bigger than those in the electride, the channel structure is markedly different, forming a 3-dimensional network. The magnetic susceptibilities of both phases of the electride above 14 K are well-fit by the linear chain Heisenberg antiferromagnetic model with values of J/k_B of −54 (crystals) and −17.8 K (powder). Both types show marked deviations below 14 K toward greater spin-pairing. This behavior was verified by EPR measurements of intensity *vs* temperature. The electride was characterized further by two probe pressed pellet conductivity, variable temperature ⁷Li MAS-NMR, and DSC.

Introduction

Electrides are crystalline salts in which the charges on complexed alkali cations are balanced by an equal number of trapped electrons.[1−8] The quest for homogeneous, crystalline electrides with well-defined properties was a long one, starting with the observation of "dark blue paramagnetic solids" upon evaporation of solutions when the first alkalide, Na+(cryptand[2.2.2])Na− was synthesized.[9,10] The optical spectra of thin films produced by solvent evaporation suggested the formation of solid electrides,[11−13] but attempts to crystallize electrides were unsuccessful until 1983 when crystalline Cs+-(18-crown-6)₂e− was prepared and characterized.[14] Several years later, its crystal structure was determined,[15,16] placing electrides on a firm footing as a new class of crystalline ionic materials in which trapped electrons serve as the anions. The crystal structures of three other electrides, K+(cryptand-[2.2.2])e−,[17,18] Cs+(15-crown-5)₂e−,[19,20] and a mixed-crown electride, [Cs+(15-crown-5)(18-crown-6)e−]₆•(18-crown-6),[21,22] were subsequently determined and related to their optical, magnetic, and electrical properties. [Note that the abbreviations (Cmno) and (mCn) will be subsequently used for (cryptand-[*m.n.o*]) and (*m*-crown-*n*), respectively.]

On the basis of both theory[23−27] and experiment,[3,28] there is now little doubt that, to first order, electrides may be viewed

(1) Dye, J. L. *Prog. Inorg. Chem.* **1984**, *32*, 327−441.

(2) Dye, J. L. In *Valency, The Robert A. Welch Foundation Conference on Chemical Research*; Robert A. Welch Foundation: Houston, Texas, 1989; Vol. XXXII, pp 65−91.

(3) Dye, J. L. *Science* **1990**, *247*, 663−668.

(4) Dye, J. L.; Huang, R. H. *Chem. Br.* **1990**, *26*, 239−244.

(5) Dye, J. L. *Chemtracts−Inorg. Chem.* **1993**, *5*, 243−270.

(6) Dye, J. L. In *Physical Supramolecular Chemistry*; Echegoyen, L., Kiefer, A., Eds.; Kluwer Academic Publishers: Dordrecht, The Netherlands, 1996; pp 313−336.

(7) Wagner, M. J.; Dye, J. L. *Annu. Rev. Mater. Sci.* **1993**, *23*, 223−253.

(8) Wagner, M. J.; Dye, J. L. Alkalides and Electrides. In *Comprehensive Supramolecular Chemistry*; Gokel, G. W., Ed.; Elsevier: Oxford, UK, 1996; Vol. 1, pp 477−510.

(9) Dye, J. L.; Ceraso, J. M.; Lok, M. T.; Barnett, B. L.; Tehan, F. J. *J. Am. Chem. Soc.* **1974**, *96*, 608−609.

(10) Tehan, F. J.; Barnett, B. L.; Dye, J. L. *J. Am. Chem. Soc.* **1974**, *96*, 7203−7208.

(11) Dye, J. L.; Yemen, M. R.; DaGue, M. G.; Lehn, J. *J. Chem. Phys.* **1978**, *68*, 1665−1670.

(12) DaGue, M. G.; Landers, J. S.; Lewis, H. L.; Dye, J. L. *Chem. Phys. Lett.* **1979**, *66*, 169−172.

(13) Dye, J. L.; DaGue, M. G.; Yemen, M. R.; Landers, J. S.; Lewis, H. L. *J. Phys. Chem.* **1980**, *84*, 1096−1103.

(14) Ellabouddy, A.; Dye, J. L.; Smith, P. B. *J. Am. Chem. Soc.* **1983**, *105*, 6490−6491.

(15) Dawes, S. B.; Ward, D. L.; Huang, R. H.; Dye, J. L. *J. Am. Chem. Soc.***1986**, *108*, 3534−3535.

(16) Dawes, S. B.; Ward, D. L.; Fussa-Rydel, O.; Huang, R.-H.; Dye, J. L. *Inorg. Chem.* **1989**, *28*, 2132−2136.

(17) Huang, R. H.; Faber, M. K.; Moeggenborg, K. J.; Ward, D. L.; Dye, J. L. *Nature* **1988**, *331*, 599−601.

(18) Ward, D. L.; Huang, R. H.; Dye, J. L. *Acta Crystallogr.* **1988**, *C44*, 1374−1376.

(19) Ward, D. L.; Huang, R. H.; Kuchenmeister, M. E.; Dye, J. L. *Acta Crystallogr.* **1990**, *C46*, 1831−1833.

(20) Dawes, S. B.; Eglin, J. L.; Moeggenborg, K. J.; Kim, J.; Dye, J. L. *J. Am. Chem. Soc.* **1991**, *113*, 1605−1609.

(21) Wagner, M. J.; Huang, R. H.; Eglin, J. L.; Dye, J. L. *Nature* **1994**, *368*, 726−729.

(22) Wagner, M. J.; Dye, J. L. *J. Solid State Chem.* **1995**, *117*, 309−317.

as "stoichiometric F-center compounds" in which the excess electron density is concentrated in the cavities and the electrons serve as the "anions" in an ionic compound. By developing new computer visualization methods that permit detailed examination of the void spaces in a crystal structure,[22,28] we were able to relate the inter-electron magnetic coupling, conductivity, and effective dimensionality of electrides to their cavity-channel structures. The diversity of behavior is quite remarkable but correlates well with the lengths and diameters of the channels. $Cs^+(15C5)_2e^-$ [20,29] and $Cs^+(18C6)_2e^-$ [29] are 1-dimensional antiferromagnets ($-J/k_B \sim 2$ and 39 K, respectively), $K^+(C222)e^-$ is an alternating chain ($-J/k_B \sim 400$ K),[29] and $Cs^+(15C5)(18C6)e^-_6 \cdot (18C6)$ contains antiferromagnetically coupled 6-membered rings of electrons ($-J/k_B \sim 400$ K).[21,22] (In these expressions, k_B is the Boltzmann constant.) The conductivity of electrides spans nearly 10 orders of magnitude, from insulator to nearly metallic.[30] Slight changes in the cavity and channel structure can vastly change the properties of electrides.[20,29,31,32] Thus, while electrides can all be considered simple "salts" of complexed alkali metals, the unusual nature of their anions leads to a wide range of behavior that can be directly related to the structure of their void spaces.

The title electride, $Li^+(C211)e^-$, was first studied in 1981 as the residue obtained by evaporating ammonia from solutions with various ratios of lithium to C211.[33] The EPR spectra, magnetic susceptibilities, and optical spectra demonstrated the presence of at least two major electron-trapping sites in various samples. Some samples showed a single peak in the susceptibility at $\sim$20 K while others had a broad maximum at 50−60 K. The EPR signal intensity showed that the latter samples contained both the "20 K site" and a second site with a larger coupling constant. The difference in behavior was attributed to differences in the mole ratio of lithium. It was unknown at that time whether two different phases were responsible or if a single phase had two sites for electrons.

Since the original publication,[33] new synthesis methods have been used that provided crystals for structure determination, but the source of the two kinds of magnetic behavior remained unclear until recently. Some samples showed a peak in the magnetic susceptibility at $\sim$20 K while others had the maximum at $\sim$60 K. In this paper we report the properties and magnetic behavior of two distinct phases of this electride and the crystal structure of one of them. The structure shows that the excess electron trapping sites (cavities) are interconnected by zigzag channels to form an infinite chain. In addition to being connected to the nearest neighbor cavity, each cavity is connected further by a somewhat smaller channel to the next nearest neighbor cavity in the chain. This is of great interest since the structure suggests essentially 1D magnetic coupling between not only the nearest neighbors in the linear chain but

also the next-nearest neighbors. The topic of second neighbor magnetic interactions, particularly when both interactions are antiferromagnetic and thus "compete", has been a field of interest recently due to the wide range of magnetic phase behavior they are expected to display.[34−42] However, not many materials with structures that suggest such interactions have been found.[43−46] The electride presented here, $Li^+(C211)e^-$, shows clear evidence of gradual spin dimerization as the temperature is decreased below about 14 K. The driving force for this dimerization is open to question. It might result from a "conventional" spin-Peierls transition caused by spin−lattice interactions that compete with a magnetic interaction characterized by a single magnetic coupling constant J_1. Alternatively, as predicted by Haldane[36] and emphasized in recent studies of $CuGeO_3$,[39−42] competing antiferromagnetic intra-chain interactions can contribute to electronically-driven spin dimerization. Since the "excess" electrons in an electride may be considered to form an "electron lattice-gas" with little spin−orbit coupling,[28] the origin of the spin-pairing in $Li^+(C211)e^-$ is open to question.

In this paper, we focus on the structure of this electride and its relation to the experimental behavior of the bulk magnetic susceptibility as a function of temperature and magnetic field.

Experimental Section

Cryptand[2.1.1] was obtained from Aldrich (98%) and was vacuum-distilled prior to use. A lithium ingot (under argon) from AESAR (99.9%) was kept in a helium-filled glovebox and subsurface samples were used to provide weighed, shiny samples of lithium metal. For the syntheses described here, a slight excess of lithium was used. The lithium and the complexant were inserted into chambers 1 and 3 respectively of the three-compartment fused silica "K-cell" (shown in Figure 1) in the glovebox and the open sidearms were closed with sealed glass tubes and Cajon Ultra-Torr connectors.[47] After removal from the glovebox and evacuation to $<10^{-5}$ Torr, the sidearms were sealed off and either ammonia or methylamine was condensed onto the lithium. The lithium solution was transferred through a fused silica frit into chamber 2 (to reduce or eliminate iron and lithium nitride contamination), the solvent was distilled off, and the sample was again evacuated to $<10^{-5}$ Torr. Chamber 1 was then removed by flame sealing.

Methylamine ($MeNH_2$) that had been distilled from Na K was distilled into chamber 3 to dissolve the cryptand and the solution was poured through the frit onto the lithium metal (chamber 2). The solution was allowed to stand for several hours at 195 K after which the methylamine was distilled out of the cell and replaced with dimethyl ether (Me_2O) that had been dried over benzophenone in the presence of excess Na K alloy to form the ketyl and dianion. The Me_2O was removed to dryness, replaced with fresh Me_2O, and evaporated to dryness again. This was done to ensure the complete removal of

(23) Allan, G.; DeBacker, M. G.; Lannoo, M.; Lefebvre, J. *Europhys. Lett.* **1990**, *11*, 49−53.

(24) Rencsok, R.; Kaplan, T. A.; Harrison, J. F. *J. Chem. Phys.* **1990**, *93*, 5875−5882.

(25) Rencsok, R.; Kaplan, T. A.; Harrison, J. F. *J. Chem. Phys.* **1993**, *98*, 9758−9764.

(26) Kaplan, T. A.; Rencsok, R.; Harrison, J. F. *Phys. Rev. B.* **1994**, *50*, 8054−8058.

(27) Singh, D. J.; Krakauer, H.; Haas, C.; Pickett, W. E. *Nature* **1993**, *365*, 39−42.

(28) Dye, J. L.; Wagner, M. J.; Overney, G.; Huang, R. H.; Nagy, T. F.; Tomanek, D. *J. Am. Chem. Soc.* **1996**, *118*, 7329−7336.

(29) Wagner, M. J. Ph.D. Dissertation, Michigan State University, East Lansing, Michigan, 1994.

(30) Moeggenborg, K. J.; Papaioannou, J.; Dye, J. L. *Chem. Mater.* **1991**, *3*, 514−520.

(31) Dye, J. L. *Nature* **1993**, *365*, 10−11.

(32) Wagner, M. J.; Huang, R. H.; Dye, J. L. *J. Phys. Chem.* **1993**, *97*, 3982−3984.

(33) Landers, J. S.; Dye, J. L.; Stacy, A.; Sienko, M. J. *J. Phys. Chem.* **1981**, *85*, 1096−1099.

(34) Anathakrishna, G.; Weiss, L. F.; Foyt, D. C.; Klein, D. J. *Physica* **1976**, *81B*, 275−284.

(35) Hatfield, W. E. *J. Appl. Phys.* **1981**, *52*, 1985−1990.

(36) Haldane, F. D. M. *Phys. Rev. B* **1982**, *25*, 4925−4928.

(37) Bonner, J. C. In *Magneto-Structural Correlations in Exchange Coupled Systems*; Willett, D. G. R. D., Kahn, O., Eds.; D. Reidel Publishing Company: Dordrecht, Holland, 1985; p 157.

(38) Chubukov, A. V. *J. Phys. Condens. Matter* **1990**, *2*, 4455−4470.

(39) Riera, J.; Dobry, A. *Phys. Rev. B* **1995**, *51*, 16098−16102.

(40) Castilla, G.; Chakravarty, S.; Emery, V. J. *Phys. Rev. Lett.* **1995**, *75*, 1823−1826.

(41) Riera, J.; Koval, S. *Phys. Rev. B* **1996**, *53*, 770−774.

(42) Büchner, B.; Ammerahl, U.; Lorenz, T.; Brenig, W.; Dhalenne, G.; Revcolevschi, A. *Phys. Rev. Lett.* **1996**, *77*, 1624−1627.

(43) Brown, D. B.; Donner, J. A.; Hall, J. W.; Wilson, S. R.; Wilson, R. B.; Hodgson, D. J.; Hatfield, W. E. *Inorg. Chem.* **1979**, *18*, 2635−2641.

(44) Chiari, B.; Piovesana, O.; Tarantelli, T.; Zanazzi, P. F. *Inorg. Chem.* **1990**, *29*, 1172−1176.

(45) Chiari, B.; Piovesana, O.; Tarantelli, T.; Zanazzi, P. F. *Inorg. Chem.* **1993**, *32*, 4834−4838.

(46) Hase, M.; Terasaki, I.; Uchinokura, K. *Phys. Rev. Lett.* **1993**, *70*, 3651.

(47) Swagelok; Available from H. E. Lennon, Inc., 24148 Research Drive, Farmington Hills, MI 48335.
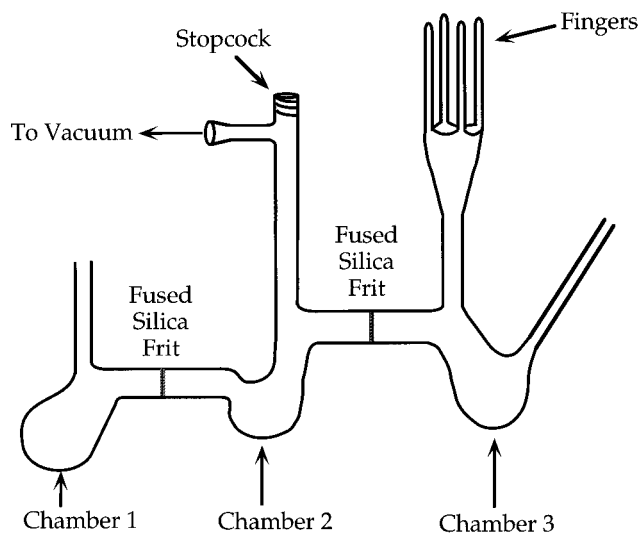
Figure 1. Three-chamber fused silica K-cell used for the synthesis of Li$^+$(C211)e$^-$.

MeNH$_2$, which can complicate the synthesis. A final fresh portion of Me$_2$O was distilled into the cell as well as enough purified diethyl ether (Et$_2$O) to create a saturated solution at dry ice temperatures. Finally the solution was poured through the frit into chamber 3 for crystallization.

Over a period of one-half to two days, the more volatile Me$_2$O was slowly allowed to distill through several frits from the solution at 195 K to a trap at liquid nitrogen temperatures. This procedure usually resulted in the growth of crystals up to 0.5 mm edge length when the initial solution contained no seed crystals. The only difference in methodology used to prepare the two different forms of electride described in this paper (referred to as "crystalline" and "powder") was that some precipitate had formed prior to the slow distillation of the solvent in the case of samples that formed the powder, while a solution with no visible precipitate was used to grow crystals. The behavior of samples prepared by rapidly cooling a saturated solution to produce powdered material was the same as that of slowly grown "powder" samples.

The crystals or powder were washed by distilling Et$_2$O from chamber 2 onto the samples and pouring the supernatant liquid through the frit. This procedure was carried out several times, after which the diethyl ether was removed by distillation and the cell was evacuated to $<10^{-5}$ Torr. Both types of sample form as black solids. The crystals have a shiny appearance and have either a "blocky" or needle-like morphology. Powdered samples have no apparent crystallinity. Because this electride is extremely subject to irreversible decomposition, the temperature was always kept at or below 223 K during synthesis and handling.

The synthesis and crystal growth of the sodide, Li$^+$(C211)Na$^-$, were similar except that an amount of sodium equivalent to that of C211 was used, along with a stoichiometric amount of lithium. The thermal stability of the sodide is much greater than that of the electride so that fewer problems with decomposition were encountered.

The dry crystals were transferred into a ramp-type depression in a cooled copper block (223 K) in a nitrogen-filled glovebag and covered with octane that had been dried with Na K. A suitable single crystal, which had been examined with a microscope that projected into the glovebag, was picked up by a glass fiber with grease on its tip and transferred under a cold nitrogen stream (213 K) onto the diffractometer.[18] During data collection, the crystal was kept in a cold (198 K) nitrogen stream. A Nicolet P3F diffractometer was used, with graphite-monochromatized Mo Kα radiation and a locally modified Nicolet LT-1 low-temperature system. Structures were solved by direct methods (SHELEX 86). Non-hydrogen atoms were refined anisotropically and hydrogen atoms were refined isotropically.

The temperature and field dependence of the susceptibility were determined first with an SHE SQUID variable-temperature susceptometer and later with two Quantum Design SQUID instruments. Specially fabricated Kel-F buckets with covers were used. For use with the Quantum Design SQUIDs, the dimensions of the bucket were chosen so that it fit within a plastic straw sample holder. Threads attached to

the bucket held it in a fixed position. Samples were maintained in the absence of air at 223 K or below at all times. After weighing the decomposed sample in a glovebox, the magnetization of the cleaned bucket was measured as a function of temperature and subtracted from the raw data to yield the sample magnetization.

Differential scanning calorimetry (DSC) was carried out with a Shimadzu DSC-50 calorimeter in hermetically sealed aluminum pans from 173 to 350 K. The press was cooled to liquid N$_2$ temperature in an N$_2$ glovebag while the pans were sealed. The entire calorimeter was enclosed in an N$_2$ glovebag with an open dewar of liquid N$_2$ to minimize humidity. The stage was cooled below 173 K prior to sample loading.

The ^{7}Li NMR spectra were measured at the MSU Max T. Rogers NMR Facility with a 9.395 T Varian VXR 400 S spectrometer that utilized a Varian VT-MAS probe. Samples were spun at 5.5 kHz, and a 3.5 μs pulse length with a 0.5 s post-acquisition delay time was used for 128 transients. A sealed glass capillary tube (1.7 mm o.d.) filled with methanol was fixed axially in the rotor for temperature determination via the magnitude of the dipolar splitting of the hydroxyl and methyl protons.[48] The rotors were loaded into the precooled (<153 K) probe from a liquid N$_2$ dewar to both store the sample and provide a dry atmosphere in the N$_2$ glovebag that enclosed the probe. Chemical shifts are referenced to aqueous Li$^+$ at infinite dilution.

Pressed powder dc conductivity measurements were made as a function of temperature with a Keithley 617 programmable electrometer. Alternating polarity, rectangular 100-mV pulses of 10-s duration were applied, and the current was measured during each pulse. Temperature was measured with a carbon-glass four-probe thermometer (Lakeshore Cryotronics, Inc. Model GR-1-100) and varied slowly by letting the 30-L dewar, in which the cell was suspended, warm from 125 to 250 K over a 48-h period.

The EPR data were collected with a Bruker ESP-300E series spectrometer, operating at X-band. The temperature was controlled to within ± 0.1 K with an Oxford 900 series continuous flow cryostat along with an ITC-4 temperature control unit and a GFS gas-shielded helium transfer tube. The g value was determined by direct measurement of the magnetic field strength and microwave frequency with an ER-035M NMR gaussmeter and an EIP-25B counter that operates at 3-12 GHz. The finger that contained the electride was brought into an N$_2$ glovebag that was then purged several times to ensure an inert atmosphere. A very small portion (<5 mg) of electride was scooped from a cold mortar into an evacuable 4 mm o.d. Suprasil EPR tube that was kept in liquid nitrogen. The EPR tube was then evacuated to $<10^{-5}$ Torr and sealed with a hot flame. The small sample size was necessary to prevent overload of the cavity, making absolute intensity measurements impossible.

Results and Discussion

As described above, two distinct phases of Li$^+$(C211)e$^-$ could be prepared, depending on the method used to form the solid. These two kinds of samples have different magnetic properties, and the structure of only one form could be determined.

A "blocky" crystal of Li$^+$(C211)e$^-$ with dimensions 0.4 × 0.4 × 0.6 mm was found to have the orthorhombic space group *Pbcn* (no. 60). Later samples, designated as "crystalline", were checked by X-ray diffraction to be certain that they had the same structure. A crystal of Li$^+$(C211)Na$^-$ with dimensions 0.3 × 0.3 × 0.4 mm belonged to the orthorhombic space group *Pna*21 (no. 33). The crystallographic data for both Li$^+$(C211)e$^-$ and Li$^+$(C211)Na$^-$ are given in Table 1. Positional and thermal parameters and selected bond distances and bond angles for the electride and positional parameters for the sodide are given in the Supporting Information.

Figure 2 shows the single molecule drawing of the complexed cation, Li$^+$(C211), in the electride. Its structure is virtually identical in the sodide and is also the same as in the normal salt Li$^+$(C211)I$^-$.[49] Figure 3 is a stereo ORTEP view of the molecular packing in the unit cell of the electride.

(48) English, A. D. *J. Magn. Reson.* **1984**, *57*, 491−493.
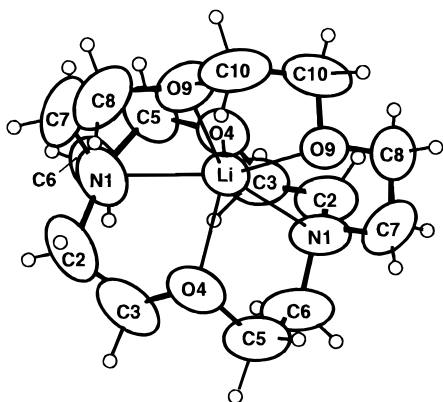(49) Moras, D.; Weiss, R. *Acta Crystallogr.* **1973**, *B29*, 400−403.

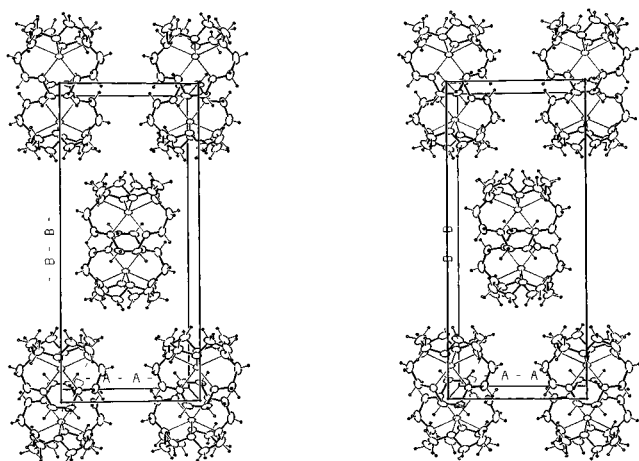**Figure 2.** Single molecule diagram of the complexed cation Li$^+$(C211) in the electride, Li$^+$(C211)e$^-$.

Figure 3. ORTEP view of the molecular packing in the unit cell of Li$^+$(C211)e$^-$.

Table 1. Crystallographic and Refinement Data for Li$^+$(C211)e$^-$ and Li$^+$(C211)Na$^-$

	Li$^+$(C211)e$^-$	Li$^+$(C211)Na$^-$
space group	*Pbcn*	*Pna*21
cell params		
a, Å	10.060(4)	9.639(5)
b, Å	23.134(8)	22.924(17)
c, Å	8.380(4)	9.6182(4)
z	8	4
crystal dimens, mm	0.4 × 0.4 × 0.6	0.3 × 0.3 × 0.4
scan type	ω	ω
maximum 2θ, deg	50	50
temp, K	198	200
no. of reflctns collected	2775	3960
no. of unique reflctns	1090	2004
no. of reflctns used in refinement with $F_o^2 > 3\sigma(F_o^2)$	617	898
no. of variables	144	226
R	0.046	0.032
R_w	0.051	0.033
high peak in final diff map, e/Å^3	0.12	0.11

As with other electrides, a dominant feature in the structure of Li$^+$(C211)e$^-$ is the presence of large cavities at which the "excess" electrons are presumably trapped. Visualization of the void spaces[22,28] permits accurate determination of the sizes and geometries of the cavities and channels in this electride. Cavities large enough to contain a sphere of diameter 4.4 Å (coordinates are *a* = 5.030 Å, *b* = 3.354 Å, *c* = 2.095 Å) are interconnected by large channels of diameter 2.4 Å and length ~3.4 Å to form a zigzag chain along *c* (see Figure 5A in ref 29). The feature that gives this electride a "spin-ladder-like" structure is a second set of channels (also in the chain along *c*) of diameter 1.5 Å
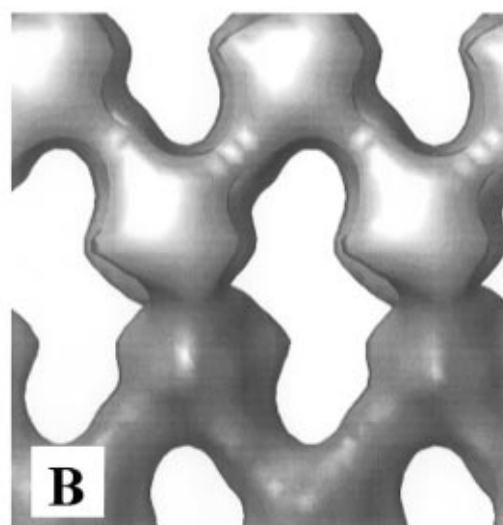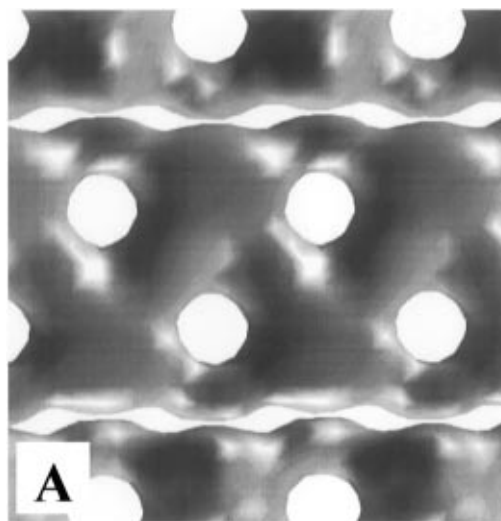

Figure 4. Views of void spaces (channels and cavities). The dark regions correspond to the boundaries of the void spaces; atoms and molecules occupy the white spaces.[29] (A) Void space isosurface for the electride, Li$^+$(C211)e$^-$, 0.55 Å from the van der Waals surfaces of the atoms. Note the two sets of channels in the chain along the *c* axis and the absence of significant inter-chain channels along the *a* axis. The sizes of cavities and channels are given in the text. (B) Void space isosurface for the sodide, Li$^+$(C211)Na$^-$, after removing Na$^-$ from the structural data set. This isosurface is 0.62 Å from the atomic surfaces. Note that zigzag channels of diameter 2.5−2.6 Å connect the 5.25 Å diameter anionic sites along both *c* and *b* (into the paper).

that connect each cavity to two next-nearest neighbors. These cavities are 8.4 Å apart, not much larger than the separation, 7.9 Å, of nearest neighbors. A view of the cavity-channel isosurface at 0.55 Å from the van der Waals surfaces of the atoms is shown in Figure 4A. Although each cavity is only 8.2 Å away from four cavities in adjacent chains, this figure makes it clear that there are no inter-chain channels of appreciable size. Such channels all have diameters smaller than 0.95 Å. In electrides, the inter-electron coupling apparently occurs primarily through the channels, rather than being determined only by distance.[28,31] Thus, we anticipate rather strong 1D antiferromagnetic coupling between electrons in adjacent cavities along the chain, weaker coupling between next-nearest neighbors along the chain, and very weak inter-chain coupling. This behavior is characteristic of 1D "ladder-like" systems (specifically the "spin frustrated double chain" described by Coronado *et al.*,[50] but with J_1 and J_2 interchanged). The sodide Li$^+$(C211)Na$^-$ is *not* isostructural with the electride as

Structure and Properties of Li⁺(Cryptand [2.1.1])e⁻

J. Am. Chem. Soc., Vol. 119, No. 16, 1997 3769

is the case with $Cs^+(15C5)_2e^-$ (and Na^-) and $Cs^+(18C6)_2e^-$ (and Na^-). Even though the structure of the complexed cation is virtually identical, the packing in the sodide is different and leads to a different arrangement of anion-trapping sites and connecting channels. These are illustrated in Figure 4B, which shows the cavity-channel structure of the sodide (obtained by removing Na^- from the crystal structure data set). In this case, the cavity diameter is somewhat larger (5.25 Å) than for the electride and each cavity is connected to four others by 2.6 Å diameter channels. Apparently, this results from a half-unit shift along c of the complexed cations in adjacent chains, so that the anionic sites in neighboring chains are not staggered as they are in the electride. The structure of the sodide yields a 3D "mesh" of anion-trapping sites and channels, very different from the 1D character of the electride. In addition, there are no second channels in the c direction of appreciable size.

No thermal transitions were observed in the electride by DSC between 173 K and the decomposition onset of ~270 K. The decomposition was very exothermic and exhibited "runaway" behavior, typical of autocatalytic decomposition.

The packed powder dc conductivity of $Li^+(C211)e^-$ from 120 to 230 K was exponential in $-1/T$ with an activation energy of 0.22 eV. As for the other electrides with "localized electrons", $Cs^+(15C5)_2e^-$ and $Cs^+(18C6)_2e^-$, this electride is essentially insulating,[30] with the observed specific conductance (~4×10^{-7} ohm^{-1} cm^{-1} at 200 K) probably caused by defect electrons or holes and diminished by grain-boundary effects.

The ^{7}Li NMR spectra of a number of samples confirm the presence of two types of samples that have different environments for Li^+. Crushed crystals show a single peak whose chemical shift varies linearly with $1/T$ from +70 ppm at 170 K to +56 ppm at 230 K. The unpaired electron contact density at Li^+, $|\psi(0)|^2$, is related to the contact (Knight) shift, $K(T)$, by[51,52]

$$K(T) = (8\pi/3N_A)\langle|\psi(0)|^2\rangle\chi(T) \tag{1}$$

in which $\chi(T)$ is the electronic contribution to the magnetic susceptibility and N_A is Avogadro's number. The magnetic susceptibility is proportional to $1/T$ in this temperature range to yield a chemical shift given by

$$\sigma(T) = \sigma(\infty) + A/T \tag{2}$$

The chemical shift extrapolated to $1/T = 0$ yields $\sigma(\infty) = -1 \pm 2$ ppm, in excellent agreement with the ^{7}Li shifts of Li^+-(C211) complexes in solution.[53] The percent atomic character of ^{7}Li due to contact density of the unpaired electron at the lithium nucleus is 0.16%, obtained by using an unpaired electron density for the gaseous lithium atom of 1.56×10^{24} e·cm^{-3}.[54] This relative contact density is about four times the value in $Cs^+(18C6)_2e^-$, probably because of the rather open faces between the long (two oxygen) and short (one oxygen) arms of the complexant.

The powder phase of $Li^+(C211)e^-$ has a different ^{7}Li NMR chemical shift that is also temperature dependent with $\sigma(\infty) = 20 \pm 2$ ppm and with 0.08% atomic character. The NMR chemical shifts of both resonances are shown as a function of $1/T$ in Figure 5. It is unlikely that the large paramagnetic shift of the powder samples at infinite temperature is due to the
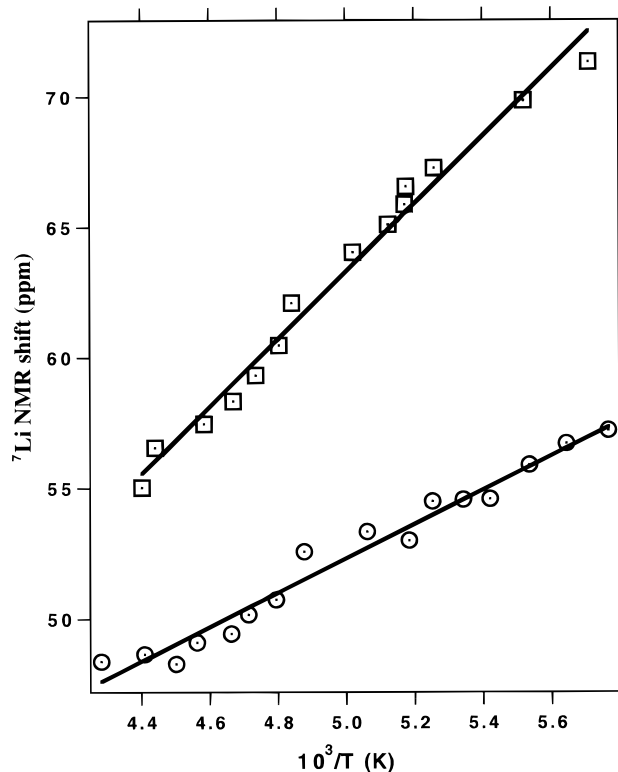
(50) Coronado, E.; Drillon, M.; Georges, R. In *Research Frontiers in Magnetochemistry*; O'Connor, C. J., Ed.; World Scientific: Singapore, 1993; p 29.
(51) Knight, W. D. *Phys. Rev.* **1949**, *76*, 1259–1260.
(52) Carrington, A.; McLachlan, A. D. In *Introduction to Magnetic Resonance*; Harper & Row: New York, 1967; p 222.
(53) Cahen, Y. M.; Dye, J. L.; Popov, A. I. *J. Phys. Chem.* **1975**, *79*, 1289–1291.
(54) O'Reilly, D. E. *J. Chem. Phys.* **1964**, *41*, 3729–3735.

Figure 5. ^{7}Li NMR Chemical shifts *vs* $1/T$ for powder (circles) and crushed crystals (squares) of $Li^+(C211)e^-$.

(typically small) Ramsey shift[55] due to Li–O contacts. It is more likely that this phase has a temperature-dependent contact density at lithium that affects the slope of σ *vs* $1/T$. For several samples, both NMR peaks were present. Decomposition leads to a single peak of Li^+ near 0 ppm.

The optical spectra of thin, solvent-free films of $Li^+(C211)e^-$ obtained by slow evaporation of ammonia were given in Figure 1 of ref 33. It now appears (see below) that the sample labeled B ($R = 1.57$) in that work is what we now refer to as the powder sample. It shows a single optical absorption peak at 2.0 μm and may have contained both powder and crystalline phases. Films obtained in the present work by evaporating dimethyl ether from a solution of the electride showed a broad peak at 1.5 μm and an extended "tail" through the visible.

The magnetic susceptibilities as a function of temperature of various preparations of $Li^+(C211)e^-$ have been measured in our laboratory by four different investigators over a time span of 15 years. It was mainly the lack of reproducibility of the susceptibility and the EPR spectra that held up publication of the structure and properties of this electride for such a long time. It is now apparent that the synthesis can lead to one or both phases of the solid and that very subtle differences in the synthesis methods are responsible. By growing crystals and checking them by X-ray diffraction before grinding them with a mortar and pestle, we were finally able to determine the properties of the form with known crystal structure. This also permitted determination of the magnetic properties of the powder phase, although its structure is not known. The original data of Landers[33] and those of three subsequent investigators can now be understood in terms of the presence of "powder-type" and/or "crystal-type" phases.

The magnetic properties of the five electrides with known crystal structures can be qualitatively related to the width, length, and shape of their anionic cavities (electron-trapping sites) and the channels that interconnect them.[28,29] This is not surprising since one might expect the excess electrons' wave functions to

(55) Ramsey, N. F. *Phys. Rev.* **1950**, *78*, 699–703.

extend into the void space between the cavities in order to minimize kinetic energy, as demonstrated theoretically for $Cs^+(15C5)_2e^-$.[27] The extent of overlap of the wave functions of neighboring electrons can thus be expected to scale with the width, length, and shape of the channels, although quantitative relations have not been developed.

As described above, the packing of the complexed cations in $Li^+(C211)e^-$ results in cavities that are connected by rather open channels in a zigzag manner. Due to the zigzag configuration, each cavity is actually nearly equidistant to its two second nearest neighbors along the chain, with, however, connecting channels that are only about half as wide. Therefore, one expects the major magnetic coupling constant (J_1) to result from nearest neighbors in the zigzag chains, with a smaller, albeit significant, coupling constant (J_2) from second-nearest-neighbor interactions. We anticipate that $J_2/J_1 < 0.25$ because of the smaller diameter and bent configuration of the channels to second nearest neighbors. Adjacent chains are probably nearly independent (magnetically), because although the distance between cavities in neighboring chains is only 4% larger than that of the nearest neighbors within each chain, no significant inter-chain channels exist.

The spin part of the Hamiltonian for an infinite chain of identical isotropic (Heisenberg) spins with first- and second-nearest-neighbor interactions is shown by eq 3 (adopting the convention for J that is common in magnetochemistry).[56]

$$\mathcal{H} = -2J_1\sum_i \hat{S}_i\hat{S}_{i+1} - 2J_2\sum_i \hat{S}_i\hat{S}_{i+2} \tag{3}$$

Use of the Heisenberg model is justified by the very small spin anisotropy (see the EPR results described below). If both interactions are antiferromagnetic, as expected for electron overlap in the channels, the nearest-neighbor interactions, which tend to align the spins antiparallel, are opposed by the second-nearest-neighbor interactions, which tend to align them parallel. Only a few "ladder-like" compounds have been reported, and no analytical solutions for the magnetic susceptibility have been found, although numerical solutions have been obtained for finite chain lengths.[39-42] Additionally, extrapolations to infinite length from exact numerical calculations on finite chains fail to converge.[34] Particularly relevant to the present case is the lack of quantitative treatments for spin-frustrated chains when J_2/J_1 is smaller than the critical value for the formation of a spin gap.

While there are no exact or approximate expressions for the magnetic susceptibility of a linear chain Heisenberg $S = {}^1/_2$ antiferromagnet with next-nearest-neighbor interactions, extrapolations to infinite chain behavior from finite size ring calculations converge when $J_2 = 0$.[57] These extrapolations fit the convenient closed form expression[58]

$$\chi_m = \frac{Ng^2\mu_\beta^2}{kT}\left[\frac{0.25 + 0.14995y + 0.30094y^2}{1 + 1.9862y + 0.68854y^2 + 6.0626y^3}\right] \tag{4}$$

in which $y = |J|/kT$ and J is constrained to be negative (antiferromagnetic). This equation is not valid at temperatures much below that at which the maximum susceptibility occurs. In addition, unlike other electrides, this electride shows a marked decrease in susceptibility as the temperature is reduced below about 14 K (see the insets to Figures 6 and 7), reminiscent of a spin-Peierls transition. There is no analytical expression for

(56) Carlin, R. L. In *Magnetochemistry*; Springer-Verlag: Berlin, 1986; p 71.
(57) Bonner, J. C.; Fisher, M. E. *Phys. Rev. A* **1964**, *135*, 640−658.
(58) Estes, W. E.; Gavel, D. P.; Hatfield, W. E.; Hodgson, D. *Inorg. Chem.* **1978**, *17*, 1415−1421.
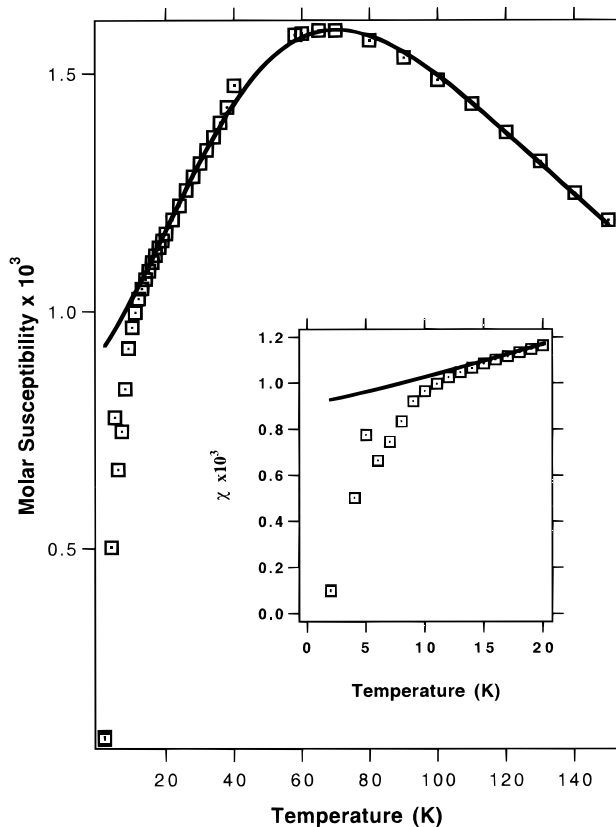

Figure 6. Magnetic susceptibility of crushed crystals of $Li^+(C211)e^-$ as a function of temperature. This run had a small contribution due to oxygen, so data points between 40 and 50 K have been deleted. The solid line is the best fit to eq 5 above 22 K, and the inset shows an expansion of the low-temperature region. The data points shown in Figures 6−8 have been corrected for the effect of the Curie Tail, and the parameters used to fit all of the data are given in Table 2.

Table 2. Susceptibility Parameters for $Li^+(C211)e^-$ Obtained by Fit of Data with Eq 5

sample	$-J/k_B$ (K)	% spins (100A)	diamagnetic correction $(-B \times 10^4)$	% Curie "tail" (100C/0.376)
crystalline	54.1	104	5.28	0.80
powder	17.8	85	5.98	1.28
mixed (crystalline)	50.3	93	2.73	0.33
mixed (powder)	16.5	7	0.43	0.13

the temperature dependence of this spin-pairing, but the intercept at 0 K should be zero. Defect electrons (in amounts that depend upon the preparation but that do not exceed 1.3%) introduce a "Curie tail" that dominates the susceptibility below about 10 K. To correct for this effect, a term C/T was subtracted from each data point with C adjusted to give the required zero intercept at $T = 0$. The "corrected" data (above $T = 22$ K for the crystalline phase and above $T = 16$ K for the powder) were then fit with a nonlinear least-squares method by the equation

$$\chi_m(T) = A\chi(y) + B \tag{5}$$

in which A, B, and J were adjusted. The values of these parameters are given in Table 2. It should be noted that the correction for the Curie tail has little effect on the values of A, B, and J. The results are shown in Figures 6−8 for various samples, and the field dependence for a crystalline sample is shown in Figure 9.

Above $T = 14$ K the fit to eq 5 is excellent and, except for the powder sample, the peak susceptibility corresponds to that expected for a stoichiometric electride ($A = 1.0$). Possible
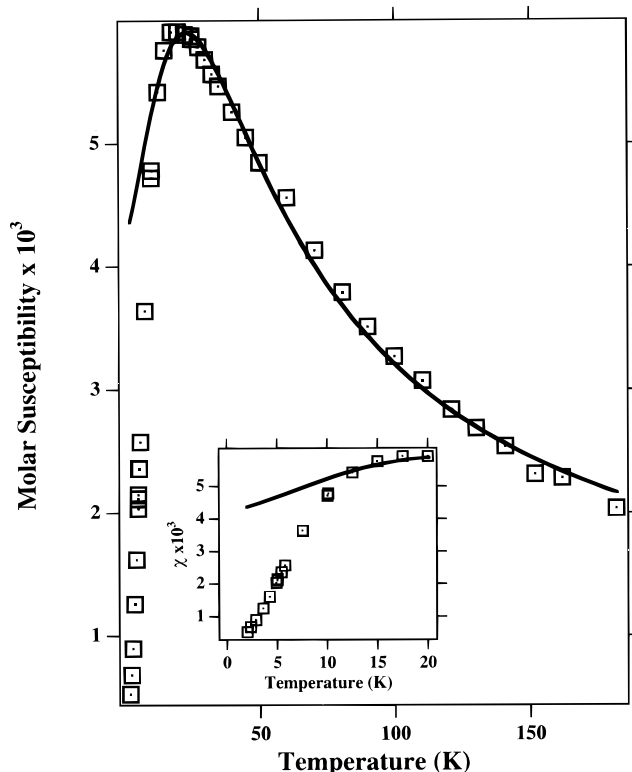
Structure and Properties of Li$^+$(Cryptand [2.1.1])e$^-$

J. Am. Chem. Soc., Vol. 119, No. 16, 1997 3771

Figure 7. Magnetic susceptibility of a powder sample of Li$^+$(C211)e$^-$ and the fit above 16 K by eq 5 (solid line). The inset shows an expansion of the low-temperature region.
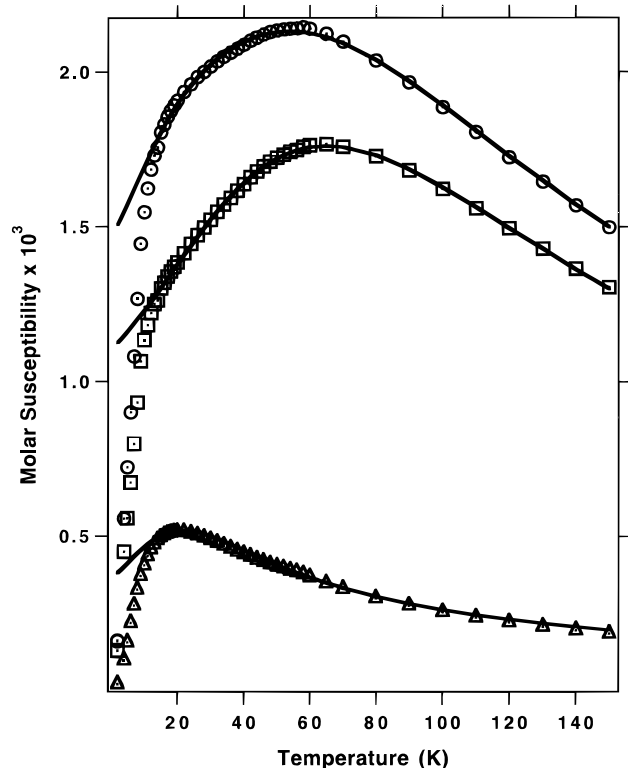

Figure 8. Magnetic susceptibility of a sample with both crystal and powder phases and the deconvolution into separate contributions by subtracting 10% of the powder phase shape shown in Figure 7. The deconvoluted data were then fit above the spin-pairing temperatures by eq 5, to yield the solid lines and the parameters given in Table 2.

reasons for the value $A = 0.85$ for the powder sample, rather than 1.0, are the following: lack of proper stoichiometry, the presence of some crystalline-phase material, or partial decomposition.
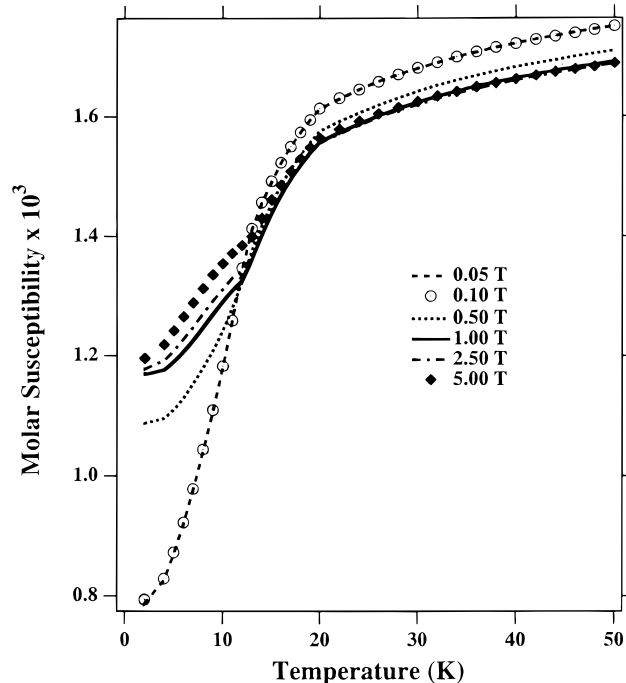

Figure 9. Magnetic field dependence of the magnetic susceptibility of a crushed crystal sample of Li$^+$(C211)e$^-$.

Although other theoretical models might also be fit to these data, our attempts to do so gave rather poor results. Of particular relevance is the value of χ_m at the maximum. This is particularly sensitive to the value of J in the LCHA model. The fact that for both the crystalline sample and the mixed sample the value of A corresponds to the total number of trapped electrons in the crystalline phase lends considerable support to this model. In addition, the validity of a 1D model is strongly supported by the chain-like geometry of the cavities and channels.

The EPR spectra of Li$^+$(C211)e$^-$ crystalline samples that are finely crushed exhibit line shapes that depend on the temperature at which the data are collected. At very low temperatures (from 4 to 10 K) the spectra have broad, weak, featureless line shapes with peak-to-peak line widths that range from 1.3 to 1.6 G. At ~10 K, a shoulder appears on the low-field side of the line, and this axial line shape feature becomes more pronounced as the temperature is increased, becoming most well-defined at about 25 K. At this temperature, $g_{||} = 2.01157$ and $g_\perp = 2.01121$. As the temperature is increased, the two features begin to coalesce until a single asymmetric line is observed at about 55 K. The exchange-narrowed line has a peak-to-peak line width of about 0.2–0.3 G. As the temperature is raised to about 170 K, the line shape does not change appreciably, but the intensity slowly decreases. When the temperature is decreased, the axial line shape begins to form again at a temperature of about 50 K, and at ~23 K the parallel and perpendicular components of the g tensor become the most pronounced with the same g values as reported above. At ~10 K, only a small shoulder remains, and this feature is completely lost below this temperature. The peak-to-peak line width is once again around 1.5 G. These results demonstrate that the changes in the EPR spectra are reversible. Details of the EPR spectra will be published separately.

Double integration of each EPR spectrum and correction for instrument gain yields the relative spin susceptibility as a function of temperature. Such data for the crystalline material are shown in Figure 10 and for powder samples in Figure 11. These data show that the spin susceptibilities have the same temperature and sample dependence as the bulk susceptibilities obtained from the SQUID measurements.
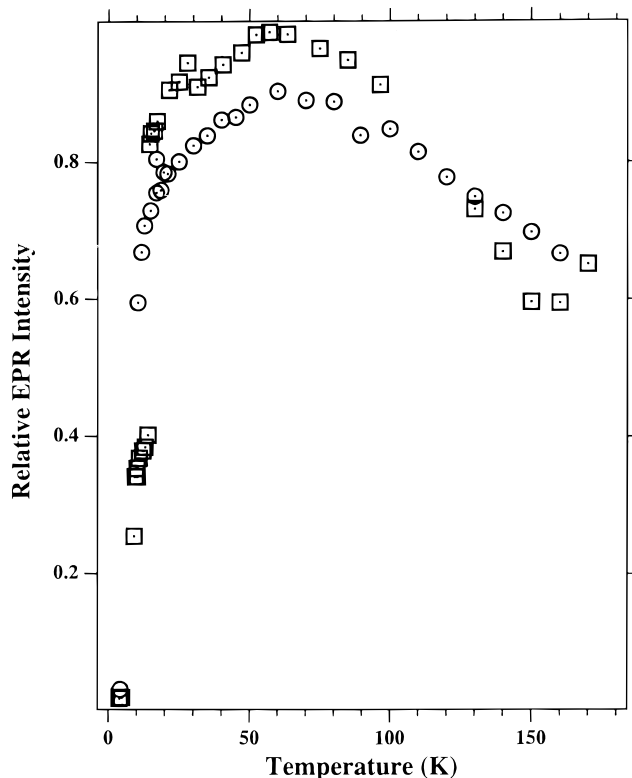
Figure 10. Relative spin susceptibility of a ground crystal sample of Li$^+$(C211)e$^-$, determined by double integration of the EPR spectrum and correction for changes in the amplification factor. Squares represent data taken during an increase in temperature, and circles are for decreasing temperature.

Conclusions

The susceptibility data and fits to eq 4 shown in Figures 6–8 and the spin susceptibilities from EPR intensities (Figures 10 and 11) show that a spin-pairing process begins at about 14 K and that the susceptibility goes smoothly to zero at 0 K upon removal of a Curie tail contribution. The fit of the data by the 1 D Heisenberg model with a single value of *J* is excellent above 14 K for both types of sample. The low-temperature drop in the susceptibility is qualitatively like that of a spin-Peierls transition, which is a manifestation of the intrinsic instability of a 1D Heisenberg chain toward dimerization. However, competition between nearest-neighbor and next-nearest-neighbor interactions may also contribute to the dimerization. The "frustration" could be relieved by redistribution of the electron density within the cavity channel framework to yield stronger pairwise interactions through the major channels, which would decrease the interaction with next-nearest-neighbor trapped electrons.

The difference between the magnetic susceptibility behavior of crystalline and powder samples is remarkable but not unprecedented. Both Cs$^+$(18C6)$_2$e$^-$ [20] and Cs$^+$(15C5)$_2$e$^-$ [32] have crystalline and disordered phases. The disordered phases show *no* susceptibility maximum, even though no appreciable decomposition accompanies the order−disorder transition. Presumably, small changes in packing drastically affect the electron−electron coupling.[31] We conclude that rapidly-formed powdered samples of Li$^+$(C211)e$^-$ or those grown from such "seeds" pack in such a way as to decrease the effective value of $-J_1/k_B$ from 54 to 18 K, probably by altering the size of the inter-connecting channels. The difference between the two
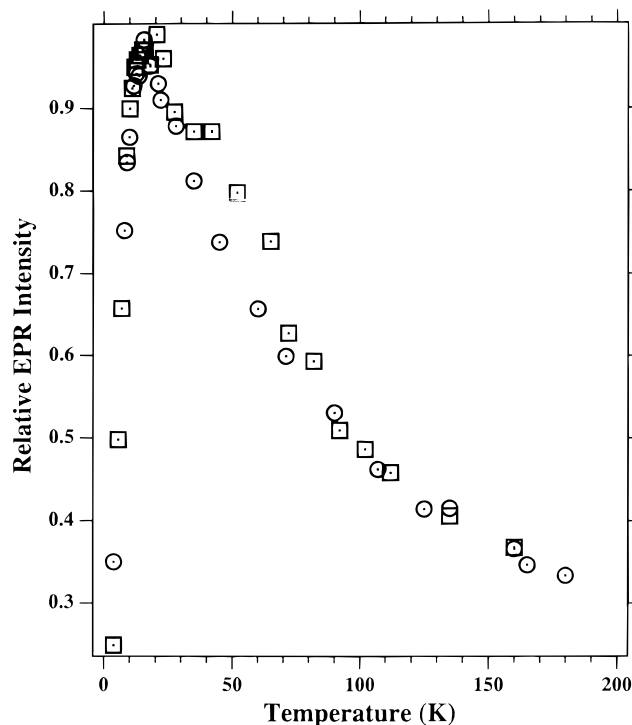
phases is also reflected by differences in the ^{7}Li NMR chemical shifts. It is curious, however, that the onset temperature of spin dimerization is nearly identical for both phases.

The field dependence of the magnetic susceptibility shown in Figure 9 may provide a clue to the dimerization process that begins at around 14 K. The uncorrected susceptibility is independent of field up to 0.1 T but shows a "knee" at 8−9 K for higher fields. This may be the result of the field stabilization of the "frustrated" state. Alternatively, it may be due to spin anisotropy. A similar field dependence below 4 K for Cs$^+$(15C5)$_2$e$^-$ was attributed[20] to a "spin-flop" in a 3D system with slight anisotropy. It is now clear that the geometry and susceptibility of Cs$^+$(15C5)$_2$e$^-$ would be more appropriately described by a 1D Heisenberg model.[29] The low-temperature "spin-flop" indicates a rather weak spin anisotropy, which causes deviations from the Heisenberg model. However, a complete understanding of the magnetic behavior of the "new" electride, Li$^+$(C211)e$^-$, in particular, and electrides in general will require new models of their electron−electron interactions.

Supporting Information Available: Tables of printed and thermal parameters of atoms, bond distances and angles, general temperature factor expressions, and torsion angles for Li$^+$-(cryptand [2.1.1])e$^-$ and positional parameters for lithium cryptand [2.1.1] sodide (5 pages). See any current masthead page for ordering and Internet access instructions.

JA9640760

Figure 11. Relative spin susceptibility of a powder sample of Li$^+$(C211)e$^-$. Squares represent data taken during an increase in temperature, and circles are for decreasing temperature.